frontiers | Frontiers in Energy Research

ORIGINAL RESEARCH
published: 22 June 2022
doi: 10.3389/fenrg.2022.811832

Chemical Analysis and Electrochemical Monitoring of Extremely Low-Concentration Corrosive Impurity MgOHCl in Molten $MgCl_2$–KCl–NaCl

Qing Gong[1], Wenjin Ding[1]*, Yan Chai[1], Alexander Bonk[1], Julian Steinbrecher[1] and Thomas Bauer[2]*

[1]Institute of Engineering Thermodynamics, German Aerospace Center (DLR), Stuttgart, Germany, [2]Institute of Engineering Thermodynamics, German Aerospace Center (DLR), Cologne, Germany

$MgCl_2$–KCl–NaCl is a promising thermal energy storage (TES) material and heat transfer fluid (HTF) with high operating temperatures of >700°C for next-generation concentrating solar power (CSP) plants. One major challenge for future implementation of the molten chloride TES/HTF technology arises from the presence of some corrosive impurities, especially MgOHCl, a hydrolysis product of hydrated $MgCl_2$. Even extremely low-concentration MgOHCl (tens of ppm O in weight) can cause unneglectable corrosion of commercial Fe–Cr–Ni alloys, which limits their service time as the structural materials in the molten chloride TES/HTF system. Thus, the chemical analysis and monitoring techniques of MgOHCl at the tens of ppm O level are vital for corrosion control. In this work, a chemical analysis technique based on direct titration and a high-precision automatic titrator was developed for an exact measurement of MgOHCl at the tens of ppm O level. It shows a standard deviation below 5 ppm O and an average error below 7 ppm O when the concentration of MgOHCl is 36 ppm O. Moreover, compared to other methods available in some literature reports, it can exclude the influence of co-existing MgO on the MgOHCl concentration measurement. This chemical analysis technique was used to calibrate the previously developed electrochemical method based on cyclic voltammetry (CV) to achieve reliable *in situ* monitoring of MgOHCl in the $MgCl_2$–KCl–NaCl molten salt at a concentration as low as the tens of ppm O level. The *in situ* monitoring technique shows a monitoring limitation of <39 ppm O. The two techniques for MgOHCl measurement developed in this work could be used to develop an *in situ* corrosion control system to ensure the long service time of the molten chloride TES/HTF system in next-generation CSP plants.

Keywords: MgOHCl concentration measurement, direct titration, cyclic voltammetry, corrosion control, next-generation concentrating solar power

OPEN ACCESS

Edited by:
Xiaohui She,
University of Birmingham,
United Kingdom

Reviewed by:
Yafei Wang,
University of Wisconsin-Madison,
United States
Brenda Garcia-Diaz,
Savannah River National Laboratory
(DOE), United States
Zhu Jiang,
Southeast University, China
Zhongfeng Tang,
Shanghai Institute of Applied Physics
(CAS), China

****Correspondence:***
Qing Gong
qing.gong@dlr.de
Wenjin Ding
wenjin.ding@dlr.de

Specialty section:
This article was submitted to Process and Energy Systems Engineering, a section of the journal Frontiers in Energy Research

Received: *09 November 2021*
Accepted: *10 May 2022*
Published: *22 June 2022*

Citation:
Gong Q, Ding W, Chai Y, Bonk A, Steinbrecher J and Bauer T (2022) Chemical Analysis and Electrochemical Monitoring of Extremely Low-Concentration Corrosive Impurity MgOHCl in Molten $MgCl_2$–KCl–NaCl. Front. Energy Res. 10:811832. doi: 10.3389/fenrg.2022.811832

INTRODUCTION

$MgCl_2$–KCl–NaCl molten chloride salt has received much attention in recent years due to its wide working temperature range (420–800°C), low vapor pressure, low material cost, and good heat capacity (Mehos et al., 2017; Ding et al., 2018a; Turchi et al., 2018; Villada et al., 2021). It has potential use in the next-generation concentrating solar power (CSP) plants as thermal energy storage (TES) material and heat transfer fluid (HTF), allowing the operating temperature of the CSP plant to be increased from about 560°C to >700°C. With such a high operating temperature, the energy efficiency of the power cycle in the CSP plant can rise from 40% to >50% when integrated with the supercritical carbon dioxide (sCO_2) Brayton power cycle, which would significantly reduce the levelized cost of electricity (LCOE) of CSP (Mehos et al., 2017). However, the molten $MgCl_2$–KCl–NaCl mixture is strongly corrosive to commercial Fe-Cr-Ni alloys even under a protective inert atmosphere (Ding et al., 2018c; Sun et al., 2018), which greatly limits its application.

Numerous studies have shown that the corrosion in molten $MgCl_2$–KCl–NaCl salt is caused by corrosive impurities, especially MgOHCl (Ding et al., 2018c; Choi et al., 2019; Grégoire et al., 2020; Sun et al., 2020; Zhao, 2020), not by the molten chloride salt itself (Zhang et al., 2020). As a consequence of the strong hygroscopicity of $MgCl_2$, some moisture is inevitably absorbed in $MgCl_2$–KCl–NaCl in practical applications. Subsequently, the main corrosive impurity MgOHCl is generated as a hydrolysis product during heating in the melting process, resulting in the strong salt corrosivity to the metallic structural materials, such as Fe–Cr–Ni alloys (Kipouros and Sadoway, 2001; Kashani-Nejad, 2005; Ding et al., 2018c). To represent the concentration of MgOHCl (*C(MgOHCl)*)in the molten salt, the unit parts per million oxygen (*ppm O*) is defined as the mass fraction of oxygen ($m_{O\ in\ MgOHCl}$) in the total mass of the salt sample (m_{sample}), as shown in **Eq. 1** (Skar, 2001).

$$\boldsymbol{C(MgOHCl)[ppm\ O] = m_{O\ in\ MgOHCl} / m_{sample} \times 10^6} \quad (1)$$

The estimated acceptable impurity level of MgOHCl for the different types of alloys based on the literature (Ding et al., 2018c; Ding et al., 2019a; Ding et al., 2019b; Kurley et al., 2019) and their relative cost factors (Gilardi et al., 2006) are summarized in **Table 1**. To allow the use of inexpensive alloys (e.g. stainless steels) for TES/HTF with molten $MgCl_2$–KCl or $MgCl_2$–KCl–NaCl at ≥700°C, the salt impurity needs to be controlled at the tens of ppm O level by monitoring and salt purification to control the salt corrosivity (Ding et al., 2019b; Kurley et al., 2019). As shown in **Figure 1**, a corrosion control system (CCS) integrated into the molten chloride TES/HTF system has been proposed in the previous work, which contains the main parts—part of online corrosion monitoring and part of corrosion mitigation (Villada et al., 2021). For CCS, reliable *in situ* and *ex situ* monitoring techniques of MgOHCl at the tens of ppm level are vital to ensure its effectiveness, efficiency, and economics.

To measure the oxygen-containing impurity concentration or redox potential of molten salts, electrochemical methods including cyclic voltammetry (CV) (Skar, 2001; Ding et al., 2017; 2018b; Choi et al., 2019; Gonzalez et al., 2020; Guo et al., 2021), square wave voltammetry (SWV) (Song et al., 2018), chronopotentiometry (CP) (Zhang et al., 2020), and open-circuit potentiometry (OCP) (Choi et al., 2019; Gonzalez et al., 2020) have been employed in molten chloride salts (Williams et al., 2021). Among them, an approach combining *in situ* and *ex situ* measurement of $MgOH^+Cl^-$ was investigated, in which cyclic voltammetry (CV) was employed as the *in situ* measurement of MgOHCl (Skar, 2001; Ding et al., 2018b; Guo et al., 2021), while *ex situ* methods of titration (Skar, 2001; Ding et al., 2018b) and carbothermal reduction (Skar, 2001) were used for the *ex situ* measurement to calibrate the *in situ* CV measurement. The reduction peak in the cyclic voltammogram—peak *B*, shown in **Figure 2**, represents the reaction of $MgOH^+$ to MgO, as shown in **Eq. 2** (Skar, 2001; Ding et al., 2018b; Guo et al., 2021). Moreover, the current density of peak B in the cyclic voltammogram is linearly linked to the concentration of $MgOH^+$.

$$\boldsymbol{MgOH^+ + e^- \rightarrow MgO(s) + \frac{1}{2}H_2(g)} \quad (2)$$

It was pointed out in the work of Skar (2001) and Ding et al. (2018b) that the *ex situ* measurements based on titration and carbothermal reduction could result in an over-measurement of the $MgOH^+$ concentration and biased calibration of CV since

TABLE 1 | Comparison of the Ni content, cost of the alloys, and their estimated acceptable impurity level with a target corrosion rate of 15 μm/year at ≥700°C for molten $MgCl_2$-KCl or $MgCl_2$-KCl-NaCl under inert atmosphere.

Alloy	Example	Ni (wt%)	Relative cost factor (compared to 3-series stainless steel)	Acceptable MgOHCl level	Data source
3-series stainless steel	SS 310 and SS 316	<30	1	Tens of ppm O	Ding et al. (2019b) Kurley et al. (2019)
Incoloy	In 800 H	30–50	~2.5	Tens of ppm O	Ding et al. (2019a) Ding et al. (2019b)
Hastelloy	Ha 276, Ha 230, and Ha N	>50	~10	Hundreds of ppm O	Ding et al. (2018c) Ding et al. (2019b) Kurley et al. (2019)

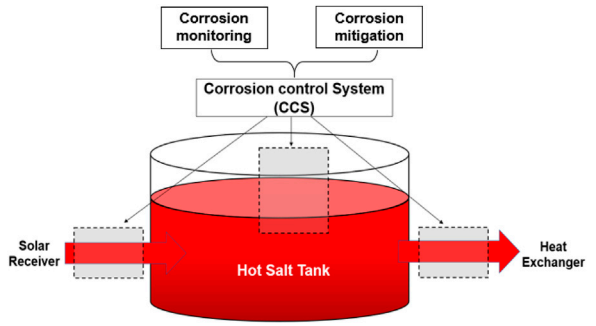

FIGURE 1 | Corrosion control system (CCS) integrated into the molten chloride TES/HTF system, which contains the online corrosion monitoring and mitigation parts, and has been proposed in the previous work (Villada et al., 2021).

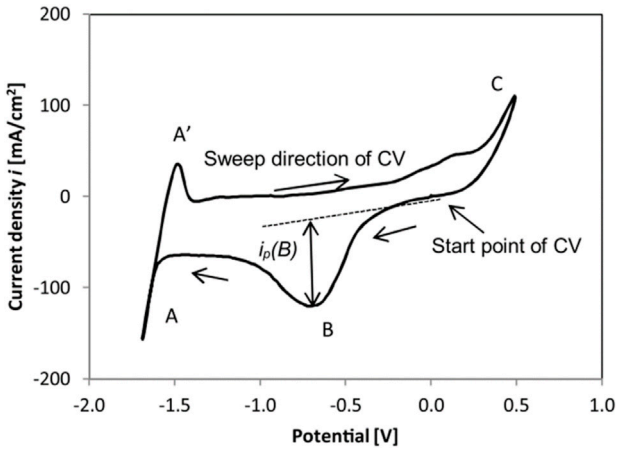

FIGURE 2 | Cyclic voltammogram in eutectic $MgCl_2$/KCl/NaCl at 500°C obtained by a tungsten working electrode with a sweep rate of 200 mV/s (Ding et al., 2017; 2018b).

other impurities (e.g. MgO or H_2O) cannot be quantitatively excluded in these *ex situ* measurements. In the $MgCl_2$-KCl-NaCl molten salt, non-corrosive MgO and corrosive MgOHCl commonly co-exist. When the temperature is >555°C, MgOHCl can be decomposed into MgO and HCl, as shown in **Eq. 3** (Kipouros and Sadoway, 2001; Kashani-Nejad et al., 2005).

$$MgOHCl \rightarrow MgO(s)+HCl(g) \quad (3)$$

To measure non-corrosive MgO and corrosive MgOHCl separately, Klammer et al. (2020) used water and methanol to extract MgOHCl/MgO based on the solubility difference (Klammer et al., 2020). This method can measure the concentration of MgOHCl down to 0.1 wt% (~200 ppm O) by a typical ethylenediaminetetraacetic acid (EDTA) titration technique and has been used to measure the purity of $MgCl_2$-containing chloride mixtures after pre-purification. However, due to the solubility of MgOHCl in methanol, this method cannot measure the extremely low-concentration MgOHCl.

In general, it was proposed that the *in situ* electrochemical CV measurement of MgOHCl calibrated by a reliable *ex situ* chemical analysis method is a promising approach to monitor MgOHCl (i.e., salt corrosivity) in molten $MgCl_2$–KCl–NaCl. However, existing electrochemical and chemical measurement methods of MgOHCl have minimum measurement limits above the acceptable MgOHCl level. For corrosion control, the MgOHCl concentration should be controlled at tens of ppm O to allow inexpensive alloys (e.g., stainless steel) to withstand the corrosion of molten $MgCl_2$–KCl–NaCl at ≥700°C. In this experiment, aiming to develop reliable chemical analysis and *in situ* monitoring techniques for MgOHCl at the tens of ppm O level, the following experiments were designed and carried out:

- Different concentrations of MgOHCl from thousands to tens of ppm O level were obtained by electrolysis at 500°C and thermal decomposition at 600 and 700°C.
- A chemical analysis technique based on direct titration and a high-precision automatic titrator was developed to measure MgOHCl concentration at the tens of ppm O level.
- The reliable concentration data on MgOHCl obtained by titration were used to calibrate the CV data to develop an *in situ* monitoring technique for MgOHCl at tens of ppm O.

EXPERIMENTAL

Materials and Experimental Setup

KCl (purity >99 wt%) and NaCl (purity >99 wt%) were purchased from Alfa Aesar, Germany, while anhydrous $MgCl_2$ (purity >99 wt%) was supplied by Magnesia, Germany. They were used to synthesize the eutectic salt mixture of $MgCl_2$-NaCl-KCl (47.1-30.2-22.7 mol%) for the experiments. This eutectic salt composition is suggested by the previous work (Villada et al., 2021).

Figure 3 shows the setup of electrochemical experiments. A chemically stable glassy carbon crucible purchased from HTW Germany (Sigradur® G) was used in this work to prevent the reaction of the strongly corrosive molten chloride salt with the crucible. The 250 g chloride salts were heated in an argon atmosphere (purity ≥99.999%, H_2O ≤ 0.5 ppm, 10 nL/h, and pressure above atmospheric pressure of about 0.1 bar) to 500°C, 600°C, or 700°C. As shown in **Figure 3**, an alumina plate was used under the glassy carbon crucible to electrically insulate the glassy carbon and the autoclave system made of steel from each other.

As shown in **Figure 3**, five electrodes were used for electrolysis and cyclic voltammetry (CV). All the electrochemical experiments were conducted using a ZENNIUM electrochemical workstation from Zahner GmbH (Germany). **Table 2** summarizes the electrodes used in different electrochemical experiments and the material composition of these electrodes. Three tungsten electrodes (1 mm diameter, purity >99.5%, purchased from Alfa Aesar) were used as working (~32 mm^2), counter (~100 mm^2), and quasi reference electrodes (~100 mm^2) for CV, while two graphite electrodes

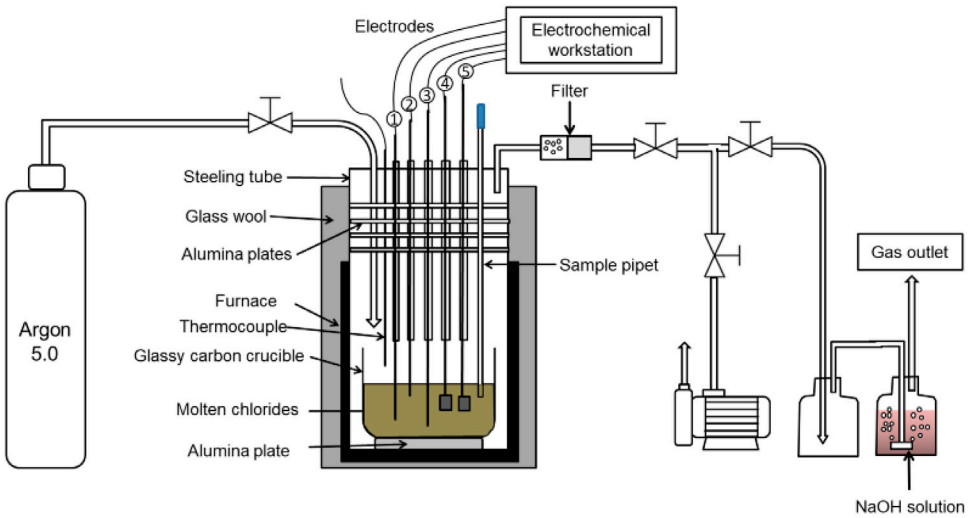

FIGURE 3 | Schematic representation of the experimental setup for electrochemical salt purification and CV experiments.

TABLE 2 | Electrodes used for electrochemical purification *via* electrolysis and monitoring the impurity concentration *via* CV.

Experiment	Application	Electrodes shown in Figure 3		
		Working	Counter	Reference
Electrolysis	Electrochemical purification	4	5	—
Cyclic voltammetry (CV)	Monitoring impurity concentration	2	3	1

1: tungsten quasi-reference electrode (~100 mm^2). 2: tungsten working electrode (~32 mm^2). 3: tungsten counter electrode (~100 mm^2). 4: graphite anode (10 mm × 40 mm) + tungsten wire for salt purification. 5: graphite cathode (10 mm × 40 mm) + tungsten wire for salt purification

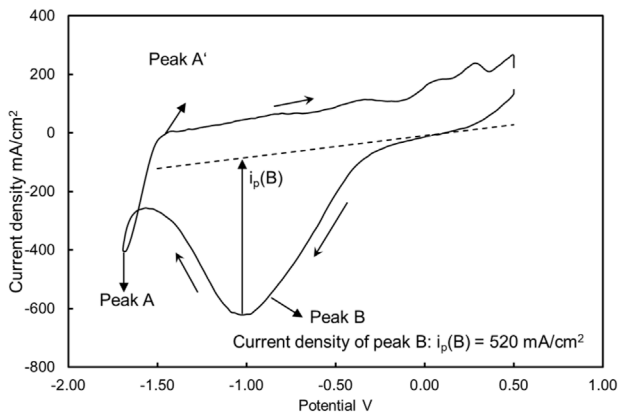

FIGURE 4 | Example of a cyclic voltammogram for molten $MgCl_2$-KCl-NaCl salt with impurity ion $MgOH^+$ at 500°C. The current density of peak B in this case was 520 mA/cm^2. The working, reference, and counter electrodes of CV were tungsten. Sweep rate: 200 mV/s.

(size: 40 mm × 10 mm x 2 mm) were used for electrochemical purification. Due to their larger surface area compared with tungsten electrodes used in our previous work (Ding et al., 2017; 2018b), graphite electrodes with a 4 cm^2 area were used to have a fast purification rate and be able to purify more salt before electrode passivation.

CV Experiments

Three groups of CV experiments at different temperatures (500°C, 600°C, and 700°C) were conducted. Once the temperature of the salt reached the target temperature, the counter electrode, reference electrode of CV, and the two graphite electrodes of electrolysis were inserted into the molten salts but without touching the crucible bottom, while the immersion depth of the working electrode of CV was fixed to 10 mm (i.e., the contact area of the tungsten electrode with the melt is about 31.4 mm^2). A sweep rate of 200 mV/s was used in all CV experiments as in the previous work (Ding et al., 2017; 2018b), while the potential voltage of CV was from 0.5 V to −1.7 V *vs.* reference.

Figure 4 is an example cyclic voltammogram of the eutectic $MgCl_2$-NaCl-KCl salt before electrolysis treatment at 500°C, in which peak B represents the reduction reaction in **Eq. 2** and is in line with the previous work (Ding et al., 2018b).

Skar (2001) and Guo et al. (2021) discovered that the peak current density of the peak B (i_p(B)) is proportional to the concentration of MgOHCl (C(MgOHCl)) in molten $MgCl_2$-NaCl or (-KCl) salts(Skar, 2001; Guo et al., 2021), which is in

accordance with the Randles–Sevcik equation (Randles, 1948; Ševčík, 1948):

$$i_p(B) = 0.4463\ \frac{(nF)^{\frac{3}{2}}}{(RT)^{\frac{1}{2}}} C^{\infty}(MgOHCl) D^{\frac{1}{2}} v^{\frac{1}{2}} \quad (4)$$

where $i_p(B)$ represents the current density of peak B in A/m^2, n is the number of electrons transferred in the reaction (n = 1 for the reduction reaction in **Eq. 2**), F is the Faraday's constant (F = 96,485.3 C/mol), R is the universal gas constant (R = 8.314 J/(Kmol)), T is the temperature of the molten salt in K, C^{∞} (MgOHCl) is the bulk concentration of MgOHCl in mol/m^3, D is the diffusion coefficient of the reacting species (here $MgOH^+$) in m^2/s, which is a function of temperature, and v is the potential sweep rate in V/s. In this study, sweep rate v is a fixed value of 0.2 V/s (200 mV/s). However, considering the limit of MgO solubility in molten $MgCl_2$-containing chloride salts (Boghosian et al., 1991), MgO was habitually saturated in this work. Hence, the equation is amended to the soluble-insoluble model of the Berzins–Delahay equation (Berzins and Delahay, 1953), as shown in **Eq. 5**.

$$i_p(B) = 0.6105\ \frac{(nF)^{\frac{3}{2}}}{(RT)^{\frac{1}{2}}} C^{\infty}(MgOHCl) D^{\frac{1}{2}} v^{\frac{1}{2}} \quad (5)$$

Eq. 5 can be simplified to **Eq. 6**, where the concentration of *C(MgOHCl) [ppm O]* is proportional to $i_p(B)$. Thus, the current density of peak B obtained from CV can be used to monitor the concentration of $MgOH^+$ impurities *in situ* in the molten chloride salts (Skar, 2001). The $k(T, D)$ in **Eq. 5** is related to the temperature, sweep rate, and diffusion coefficient of the CV measurement, as shown in **Eq. 7**, where $c_2 = 3.3 \times 10^{-2}$ (ppm Ocm^3·mV ^{½})/(mAK^{½}·s) is calculated with a fixed sweep rate of 200 mV/s, *R, F,* and n in **Eq. 5**.

$$C(MgOHCl)\ [ppm\ O] = k(T, D).i_p(B) \quad (6)$$

$$k(T, D) = c_2\left(\frac{T}{Dv}\right)^{\frac{1}{2}} \quad (7)$$

In the CV experiments, all current densities of peak B were read with a tangent at the starting point of peak B as the baseline (see **Figure 4**). The current densities of peak B would then be calibrated using an advanced titration process (see *Titration Experiments* section) to improve the measurement accuracy and precision of CV.

In order to study the relationship between the current density of peak B and the concentration of MgOHCl in the molten salt (i.e., calculating the $k(T, D)$ in **Eq. 6**), the different concentrations of MgOHCl were achieved by electrolysis and thermal decomposition. In this work, different concentrations of MgOHCl at 600 and 700°C were obtained through thermal decomposition during a certain waiting time since MgOHCl decomposes to MgO and HCl at temperature >555°C, as shown in **Eq. 3** (Kipouros and Sadoway, 2001; Kashani-Nejad et al., 2005). As the heating time increased, the concentration of MgOHCl in the molten salt gradually decreased. At 500°C, different MgOHCl concentrations were obtained through electrolysis. For electrolysis, the voltage between the working electrode and counter electrode was 1.7 V, preventing the formation of Mg at a voltage higher than 1.7 V (see Peak A in **Figure 4**). The corrosive MgOHCl impurity was decomposed by electrolysis:

$$Cathode\ (Reduction):\ 2MgOH^+ + 2e^- \rightarrow 2MgO(s) + H_2(g) \quad (8)$$

$$Anode\ (Oxidation):\ Cl^- \rightarrow Cl_2(g) + 2e^- \quad (9)$$

Figures 5A,B show the flowchart of CV experiments at 500, 600, and 700°C. Cyclic voltammograms were obtained at different temperatures and different MgOHCl concentrations. After each CV experiment, 1–2 g chloride salts, as shown in **Figure 5C**, were taken out from the crucible using a sample pipet (see **Figure 3**) for further titration experiments. During the short sample extraction, the system remained under an Ar (purity: 99.999%) atmosphere all the time to avoid air leakage into the autoclave. Combining the data on titration and CV experiments, $k(T, D)$ is determined.

Titration Experiments

The acid consumption method based on titration was used for the quantitative measurement of the total amount of MgOHCl in a salt sample. A high-precision automatic titration instrument, *905 Titrando,* purchased from *Metrohm Germany,* was employed. The titration method is as follows: first, about 500 mg sample was weighed by using an analytical balance. Then, the solid samples were dissolved in a beaker with 150 ml of ultrapure water (HiPerSolv, VWR, Germany). After installation of the beaker with samples, the standard titrant (0.01 M HCl) was charged into a 20 ml cylinder from the reagent bottle and then dripped into the salt solution through the rotation of the gear at an average rate of 0.2 ml/min (slower at pH values near 7). Meanwhile, a stirrer homogenized the solution. The titration was performed under a nitrogen purge to exclude any interference from carbon dioxide/carbonic acid. Hydrochloric acid solution (0.01 M) purchased from Merck KGaA was used to prepare the standard titrant. The titer of the HCl solution was calibrated with sodium carbonate (Na_2CO_3). The pH value and the amount of the consumed titrant were plotted by the computer, as shown in **Figure 6**. The equivalence point (EP) is marked out, where moles of acid (HCl) and moles of base (MgOHCl) neutralize each other, as shown in **Eq. 10**.

$$MgOH^+(aq.) + H^+(aq.) \rightarrow Mg^{2+}(aq.) + H_2O(l) \quad (10)$$

$$C(MgOHCl)[ppm\ O] = ti \times C_{HCl} \times V_{HCl} / m_{sample} \times M_O \times 1000 \quad (11)$$

The concentration of MgOHCl in samples in ppm O is calculated according to **Eq. 11**, where *ti* is the titer of HCl, i.e., the ratio of actual concentration to theoretical concentration (0.01 M); V_{HCl} is the volume of HCl at EP in mL; C_{HCl} is 0.01 mol/L; m_{sample} is the mass of the salt sample in g, M_O is the molar mass of oxygen, i.e., 16 g/mol.

Error Analysis for Titration and CV

For *ex situ* direct titration to measure the concentration of MgOHCl in 500 mg samples, there are two main sources of error: one caused by the co-existing MgO impurity in the salt

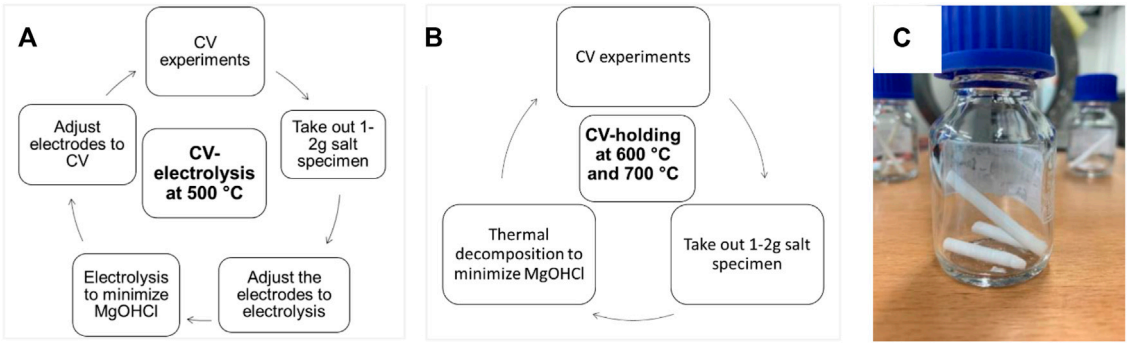

FIGURE 5 | Flowchart of CV experiments at **(A)** 500°C, **(B)** 600, and 700°C; **(C)** salt specimen taken from the glassy carbon crucible for titration.

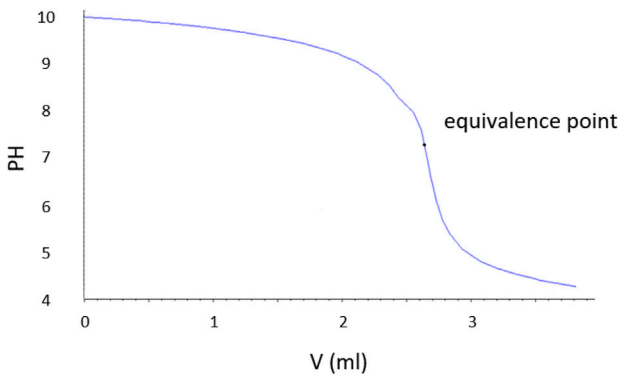

FIGURE 6 | Typical pH change curve of a direct titration of a salt sample containing MgOHCl with the 0.01 M HCl titrant recorded by using the high-precision titrator.

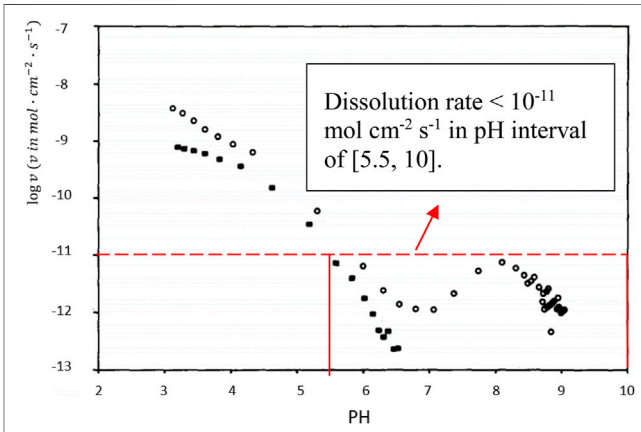

FIGURE 7 | pH *vs*. the rate of dissolution of MgO powder (°) and a (100) MgO crystal (■) at 25°C in aqueous solution (Fruhwirth et al., 1985). The dissolution rate is smaller than 10^{-11} mol cm^{-2} s^{-1} in the pH interval of [5.5, 10].

sample and another caused by the titration experiment (i.e., titration conditions and equipment).

For the first error, once the $MgCl_2$-KCl-NaCl-(MgO-MgOHCl) sample is placed in water, two types of impurities will dissolve in the water or react with water, as shown in **Eq. 12** and **Eq. 13** (Chen et al., 2018; Klammer et al., 2020).

$$MgOHCl \rightarrow Mg^{2+} + OH^{-} + Cl^{-} \quad (12)$$

$$MgO + H_2O \rightarrow Mg^{2+} + 2OH^{-} \quad (13)$$

Empirically, the dissolution of MgOHCl in water (see **Eq. 12**) occurs rapidly, when the aqueous solution is not saturated with $Mg(OH)_2$ (i.e., pH < 10.4) (Dong et al., 2010). In this work, the pH value of the salt solution for titration was smaller than 10 because of the low MgOHCl concentration (<4000 ppm O in salt samples), as shown in **Figure 6**. Unlike the rapid dissolution of MgOHCl shown in **Eq. 12**, the reaction between MgO and H_2O shown in **Eq. 13** has been experimentally proved slow in an alkali or a neutral environment, as shown in **Figure 7** (Fruhwirth et al., 1985). As can be seen, in the pH range of 6–9, the dissolution rate of MgO is less than 10^{-11} mol cm^{-2} s^{-1}. Thus, when we know the diameter and concentration of MgO particles in the system, the amount of HCl consumed by MgO can be estimated. Taking the highest concentration of MgOHCl (4000 ppm O) as a reference, the maximum mass fraction of MgO was 1 wt% (assuming that all MgOHCl was converted to MgO) (Zhao, 2020). We measured the diameter of MgO in $MgCl_2$-KCl-NaCl and found that the broad peak of the laser-based particle-size analyzer was 10–30 μm. Using the parameters mentioned earlier and the density of MgO (3.58 g/cm^3), the total surface area (A) in 250 g of chloride salt can be calculated, as shown in **Table 3**. Then, the maximum dissolution rate of MgO in this direct titration experiment can be calculated according to **Eq. 14**.

$$E = \frac{k.A.M_o}{m_s} \times 60 \times 2 \times 10^6 \quad (14)$$

where E is the error caused by MgO in ppm O/min; k is the MgO dissolution rate, adopting 10^{-11} mol cm^{-2} s^{-1}; A is total MgO surface area in cm^2, listed in **Table 3**; M_O is the molar mass of oxygen, i.e., 16 g/mol; m_s is the total salt mass, 250 g; *60* is the factor of second to minute; *2* means one MgO equivalent to two MgOHCl in titration; and 10^6 is the factor of ppm.

TABLE 3 | Error caused by the dissolution of MgO with different particle sizes in an aqueous solution with pH 5.5–10.4.

Salt mass in g	Maximum MgO fraction in wt%	MgO particle diameter (D) in μm	Total MgO surface area (A) in cm^2	Dissolution rate (k) in mol/(Cm^2 s)	Maximum error (E) in ppm O/min
250	1	10	4190	10^{-11}	0.32
250	1	20	2095	10^{-11}	0.16
250	1	30	1397	10^{-11}	0.10

TABLE 4 | Thirteen times direct titration experiments with the standard $Mg(OH)_2$ solution to determine RSD and relative error at a concentration equivalent 36 ppm O in 500-mg salt sample.

C($MgOH_2$) in mol/L	Volume in ml	V (0.01 M HCl) in ml (theoretical)	V (0.01 M HCl) in ml (titration)	Equivalent MgOHCl ppm O in 500 mg salt sample (theoretical)	Equivalent MgOHCl ppm O in 500 mg salt sample (titration)	Relative error %
1.13×10^{-5}	50	0.11	0.1381	36	44	23.15
1.13×10^{-5}	50	0.11	0.1363	36	44	21.54
1.13×10^{-5}	50	0.11	0.1522	36	49	35.72
1.13×10^{-5}	50	0.11	0.1291	36	42	15.12
1.13×10^{-5}	50	0.11	0.1418	36	46	26.45
1.13×10^{-5}	50	0.11	0.1244	36	40	10.93
1.13×10^{-5}	50	0.11	0.1285	36	41	14.59
1.13×10^{-5}	50	0.11	0.1583	36	51	41.16
1.13×10^{-5}	50	0.11	0.1246	36	40	11.11
1.13×10^{-5}	50	0.11	0.1384	36	45	23.42
1.13×10^{-5}	50	0.11	0.1090	36	35	−2.80
1.13×10^{-5}	50	0.11	0.12	36	38	4.06
1.13×10^{-5}	50	0.11	0.1280	36	41	14.14

The calculated error caused by MgO in ppm O/min is listed in **Table 3**. In the direct titration, the time required for the titration to reach EP was not exceeded by 5 min for neutralization of 50 ppm O MgOHCl by 0.01 M HCl, which means that the titration error due to co-existing MgO is less than 1.6 ppm O (0.32 × 5) for the MgOHCl concentration measurement.

The second error source of the measurement based on direct titration in this work was the experimental error, which could be caused by the dissolved carbon dioxide (i.e. carbonic acid) and the fluctuation of the HCl amount injected by gear etc. An experiment was carried out to determine the relative standard deviation (RSD) and percentage error of direct titration. An amount of 1.308 mg of $Mg(OH)_2$ was weighed and dissolved in 2 L distilled water as the 1.13×10^{-5} mol/L $Mg(OH)_2$ standard solution. Then, about 50 ml of standard solution was extracted and measured by direct titration, whose HCl consumption is equivalent to 36 ppm O MgOHCl in the 500 mg salt sample. The titration of the standard solution was repeated 13 times to obtain sufficient data for statistical analysis (see **Table 4**). It was found that the average standard deviation was 4.35 ppm O (RSD = 10.2%), and the average error was +6.62 ppm O (average relative error = +18%) for measuring the equivalent of 36 ppm O MgOHCl in 500 mg samples by direct titration using the titrator. Compared to this error, the titration error due to MgO is much smaller and thus neglectable.

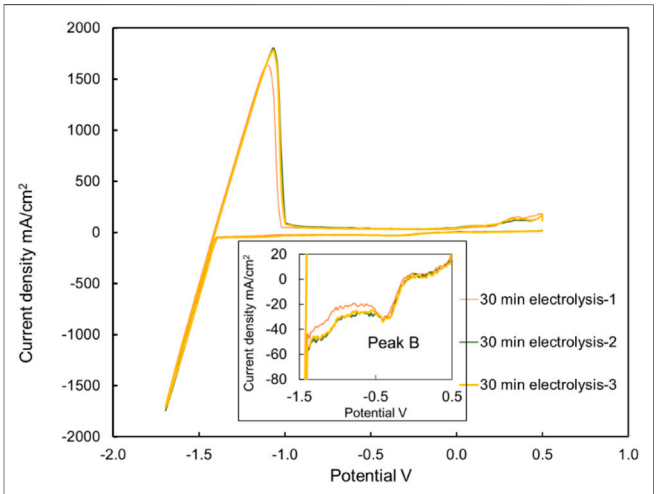

FIGURE 8 | Three cyclic voltammograms with the same molten salt batch were carried out directly and immediately after each other. The current densities of peak B were 43, 39, and 44 mA/cm^2 in three measurements, respectively. Temperature: 500°C, after 30 min electrolysis. Working, reference, and counter electrodes of CV: tungsten. Sweep rate: 200 mV/s.

For *in situ* measurement by CV, the repeatability of cyclic voltammograms is significant to determine the current density of peak B and link it to the concentration of MgOHCl. **Figure 8**

TABLE 5 | Summary of the precision and accuracy for direct titration and CV. Data on direct titration come from repeated titration of 36 ppm O equivalent MgOHCl; data on CV come from repeated scanning of 500°C salts after 30-min electrolysis.

Measurement method	Absolute error	Relative error (accuracy) %	Standard deviation	Relative standard deviation (RSD, precision) %
Direct titration	+6.62 ppm O	+18 (at 36 ppm O)	4.35 ppm O	10.2 (at 36 ppm O)
CV	Calibrated by direct titration	Calibrated by direct titration	2.65 mA/cm^2	6.3 (at 42 mA/cm^2)

displays three times the CV curves in molten chloride salt at 500°C after 30 min of electrolysis at 1.7 V. The difference of $i_p(b)$ in the same situation is the deviation of the current density. The average height of peak B is 42 mA/cm^2, while the relative standard deviation (RSD) is 6.3%, showing good stability at the low current density of $i_p(b)$. Generally, the closer to the detection limit, the greater will be the relative standard deviation. The 42 mA/cm^2 height of peak B is the smallest current density obtained at 500°C. Due to the thermal decomposition of MgOHCl (**Eq. 3**), the CV voltammograms at 600 and 700°C are not suitable for error analysis. The MgOHCl concentration changed during several CV measurements at 600 and 700°C. Hence, for all the CV measurements in this work, the relative standard errors are set at 6.3%.

Both precision and accuracy data in this work are summarized in **Table 5**. To determine the MgOHCl concentrations in salt samples and their errors, three titrations were carried out for each sample. When the standard deviation of one batch of samples was higher than 6.62 ppm O (the average error), the standard deviation of three titrations was adopted as the main error source. When the standard deviation was smaller than 6.62 ppm O, the average error (6.62 ppm O) was adopted as the domination error for the direct titration.

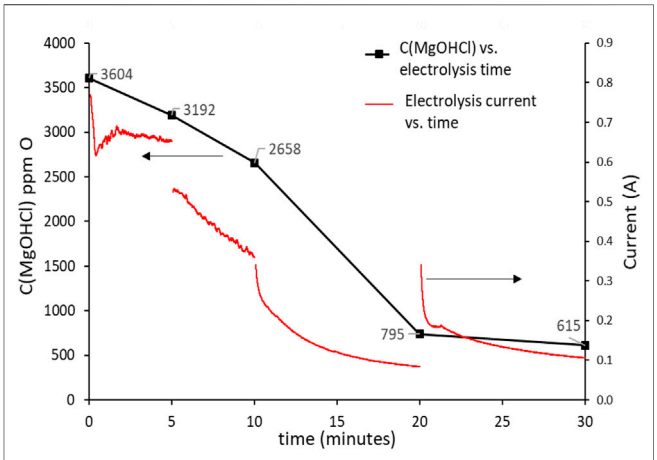

FIGURE 9 | Concentration of MgOHCl at 500°C decreases with the increasing electrolysis time. The black line using the left *y*-axis shows the concentration of MgOHCl in ppm O; the red line using the right *y*-axis shows the electrolysis current in A.

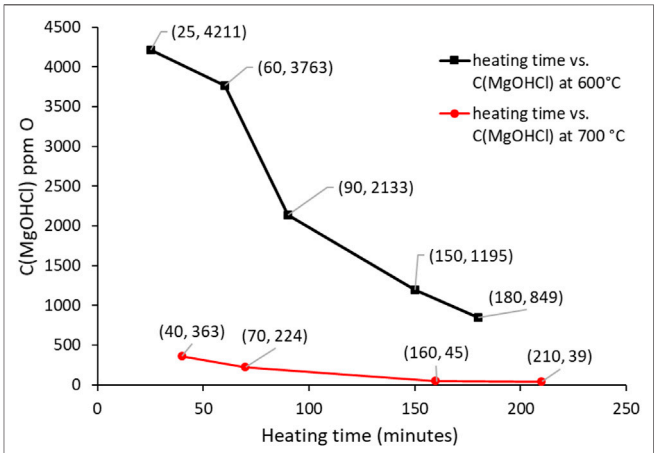

FIGURE 10 | Concentration of MgOHCl decreases with increasing holding time at 600 and 700°C.

RESULTS AND DISCUSSION

In previous work, some efforts have been made to understand the relation between the height of peak B (in **Figure 2**) and the concentration of MgOHCl in the $MgCl_2$-containing chloride salts (Skar, 2001; Ding et al., 2017; 2018b; Choi et al., 2019; Gonzalez et al., 2020; Guo et al., 2021). It was found that adding NaOH can increase the height of peak B because of the reaction shown in **Eq. 15**. In addition, the potential difference between peak B and peak A is comparable ~1.5 V. The reactions corresponding to peak A and peak A' are seen as the typical peaks of Mg^{2+} reduction and its reverse reaction of Mg oxidation, as shown in **Eq. 16** and **Eq. 17**, respectively, which can be seen as a marker. This evidence suggests that the peak at the potential of about 0 V in this work can be seen as the peak B corresponding to the reaction shown in **Eq. 2**. Different from the previous work (Ding et al., 2018b; Guo et al., 2021), the gradient of the MgOHCl concentration in this work was not obtained by adding NaOH but was obtained by electrolysis and thermo-decomposition to decrease the concentration of MgOHCl. Hence, the concentration of MgOHCl in this work was reduced to tens of ppm O since this level was interesting for corrosion control.

$$Mg^{2+}+OH^- \rightarrow MgOH^+ \quad (15)$$

$$\text{Peak A}: Mg^{2+}+2e^- \rightarrow Mg \quad (16)$$

$$\text{Peak A}': Mg \rightarrow Mg^{2+}+2e^- \quad (17)$$

Concentration of MgOHCl Measured by Titration

The decrease in the MgOHCl concentration with electrolysis time at 500°C is shown in **Figure 9**, while the decrease in the MgOHCl concentration by thermal decomposition at 600 and 700°C with enhanced holding time is displayed in **Figure 10**. All the concentration data in **Figures 9**, **10** were obtained by the direct titration method.

Figure 9 shows the relationship between the concentration of MgOHCl and electrolysis time. Generally, the concentration of MgOHCl decreased with the increasing electrolysis time at 500°C. However, as can be seen from the red line in **Figure 9**, the first two electrolysis experiments were carried out for 5 min, with the decrease in current from ~700 to ~400 mA, while the last two electrolysis experiments were conducted for 10 min with the decrease in current from ~400 to ~100 mA because of the MgO passivation. During the running of electrolysis, the poor electrical conductivity of MgO was generated, as shown in **Eq. 8**, which covered the surface of the graphite electrode and hindered electronic transmission, leading to the low efficiency of MgOHCl removal (Ding et al., 2019a). Two methods were carried out in order to mitigate the problem of the passive MgO film on the electrode and increase the efficiency of electrolysis. First, the positive and negative electrodes of electrolysis were reversed after each electrolysis. Once reversing the cathode and anode, an instantaneous recovery was displayed on the current curve, which could be attributed to the disruption of the MgO film by the generated chlorine gas (Ding et al., 2021). The reversing electrodes did not completely solve the problem of electrode passivation. Hence, second, after the first two times of 5-min electrolysis, the duration of electrolysis time was expanded to 10 min to obtain a measurable reduction of MgOHCl at lower currents.

Compared to our previous work (Ding et al., 2017), the electrolysis electrodes were improved. The tungsten wire electrodes were replaced by 10 mm × 40 mm graphite foils. After 30 min of electrolysis, the MgOHCl concentration decreased from 3603 ppm O to 415 ppm O, i.e., the concentration of MgOHCl was reduced to about 17% of the original concentration. In our previous work (Ding et al., 2017), after 25 min of electrolysis with a tungsten wire electrode, the concentration of $MgOH^+$ was reduced to only 69% of the original $MgOH^+$ concentration (from 10,400 ppm O to 7200 ppm O).

At 600 and 700°C, the reason for the decrease of MgOHCl with increasing heating time is the thermal decomposition of MgOHCl (Kipouros and Sadoway, 2001). Furthermore, the impurity level at 600°C was significantly higher than at 700°C because MgOHCl decomposes faster at 700°C than at 600°C, which compares well with that reported in some literature reports (Kashani-Nejad, 2005; Kashani-Nejad et al., 2005). In addition, before molten chloride salt reached 700°C, thermal decomposition had already occurred at the temperature range between 600 and 700°C during heating with a 5 K/min rate.

For comparison, **Table 6** lists different measurement methods of MgOHCl in molten $MgCl_2$-containing chlorides (Skar, 2001; Ding et al., 2017, 2018b; Kurley et al., 2019; Klammer et al., 2020). Kurley et al. (2019) carried out the method of direct titration to measure oxygen-containing impurities in the salt samples, which were purified by CCl_4 bubbling with as low as 1.6 ppm O impurity. This indicates that direct titration is suitable for the low concentration impurity determination of the molten chloride salt. However, the authors did not discuss the error based on their results nor did they explain the principle of direct titration to measure MgOHCl in $MgCl_2$-containing salt. In this study, it was confirmed that direct titration can measure the tens of ppm O level MgOHCl with acceptable errors. In addition, this method can exclude the interference of MgO with a relatively uncomplicated method, compared with the method published by Ding et al. (2018b) and Klammer et al. (2020). Therefore, it has relatively higher precision than the back-titration employed in our previous work (Ding et al., 2017; 2018b).

CV Results

As shown in **Figures 11–13**, the cyclic voltammograms in this work show similar features to those in the literature (Ding et al., 2018b; Choi et al., 2019; Guo et al., 2021). For example, the potential of peak B is about 1.5 V higher than that of peak A at 500–700°C. Although the height of peak A′ is not relevant to the MgOHCl concentration, it is still noticeable that the heights of oxidation peaks are different from each other. Peak A′ corresponds to the oxidation of Mg to Mg^{2+}, as shown in **Eq. 17**. This can be explained by the fact that the amount of deposition Mg on the tungsten electrodes increased as the experiment proceeded, resulting in reaction enhancement at peak A'. When the MgOHCl concentration in melts was relatively high, the deposition Mg can react with MgOHCl rapidly, as shown in **Eq. 18**. After electrolysis or decomposition, the MgOHCl concentration decreased significantly, resulting in a slower reaction of **Eq. 18** and more Mg deposition on the electrodes. This deposition of Mg could cause the high peak A'.

$$\boldsymbol{MgOHCl}(\boldsymbol{l})+\boldsymbol{Mg}(\boldsymbol{s}/\boldsymbol{l}) \rightarrow \boldsymbol{MgO}(\boldsymbol{s})+\boldsymbol{MgCl_2}(\boldsymbol{l})+\boldsymbol{H_2}(\boldsymbol{g}) \quad (18)$$

Comparing the concentrations shown in **Figure 9** and the heights of peak B shown in **Figure 11**, it is clearly visible that the height of peak B decreases from 453 to 42 mA/cm^2, with the decreasing concentration of MgOHCl from 3640 to 615 ppm O at 500°C with 30-min electrolysis at 1.7 V. Similarly, comparing the heights of peak B in **Figures 12**, **13**, with the decomposition of MgOHCl, the heights of peak B decreased significantly at 600 and 700°C as well. After 180 min of holding in the furnace under an argon atmosphere at 600°C, the current density of peak B decreased from 507 to 69 mA/cm^2, corresponding to the concentration of MgOHCl decreasing from 4211 to 894 ppm O as seen from the black line in **Figure 10**. At 700°C, after 210 min of holding, the current density of peak B decreased from 166 to 24 mA/cm^2, which corresponds to 363 and 39 ppm O MgOHCl (the red line in **Figure 10**). In general, the height of peaks B in this work always decreases with the decline in the MgOHCl concentration measured by titration.

It is a promising method to measure the MgOHCl concentration *in situ* with the current density of peak B on

TABLE 6 | Comparison with measurement methods of MgOHCl in molten chlorides.

Measurement method	Separate measurement of MgOHCl and MgO	Minimum detection limit	Measurement accuracy ppm O	Data source
Carbothermal reduction–acid consumption–iodometric titration	Yes	>70 ppm O	±20	Skar, (2001)
Extraction-EDTA titration	Yes	>200 ppm O	±40 (0.02 wt% MgOHCl)	Klammer et al. (2020)
Direct titration	Yes	~1.6 ppm O	(not analyzed)	Kurley et al. (2019)
Back titration	No	>200 ppm O	~200	Ding et al. (2017) Ding et al. (2018b)
Direct titration using a high-precision automatic titrator	Yes	~36 ppm	~6.62	This work

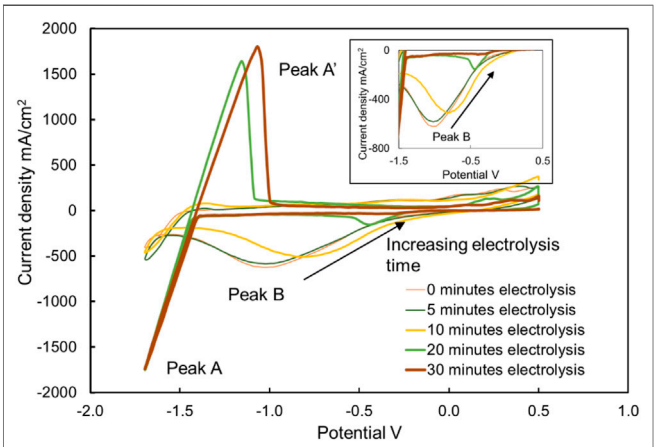

FIGURE 11 | Cyclic voltammograms of chloride molten salt before electrolysis (i.e., 0 min), after 5, 10, 20, and 30 min of electrolysis at 500°C. The working, counter, and reference electrodes of CV with a sweep rate of 200 mV/s were tungsten. The working and counter electrodes of electrolysis were graphite. The voltage on the working and counter electrodes of electrolysis was kept at −1.7 V.

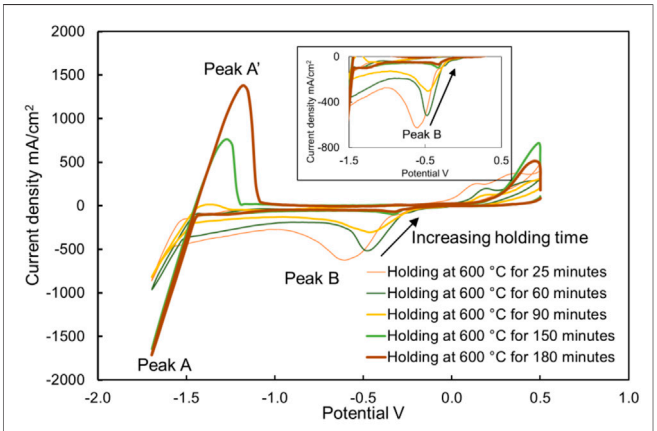

FIGURE 12 | Cyclic voltammograms of chloride molten salt, holding at 600°C for 25, 60, 90, 150, and 180 min. The working, reference, and counter electrodes of CV were tungsten. Sweep rate: 200 mV/s.

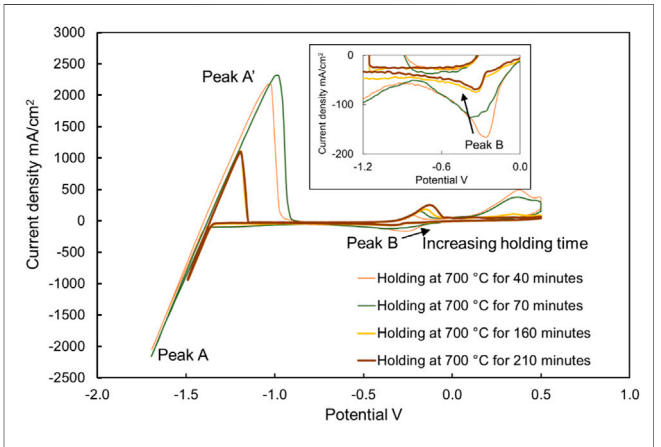

FIGURE 13 | Cyclic voltammograms of chloride molten salt, holding at 700°C for 40, 70, 160, and 210 min. The working, reference, and counter electrodes of CV were tungsten. Sweep rate: 200 mV/s. There is a correlation between the current density and impurity concentration.

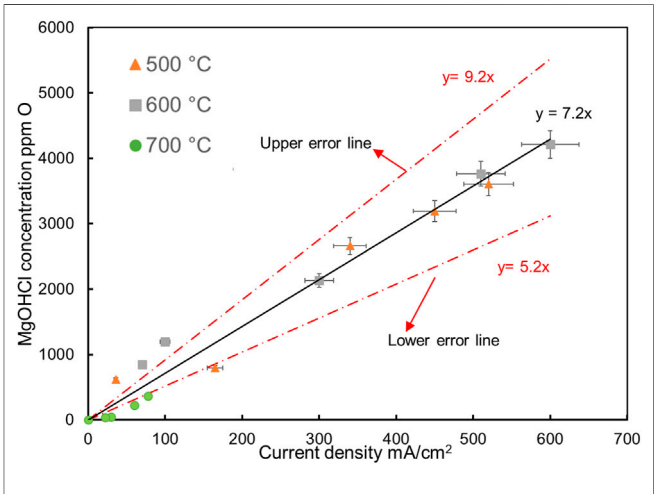

FIGURE 14 | Peak B current densities *vs*. concentrations of MgOHCl in molten $MgCl_2$-NaCl-KCl (47.1-30.2-22.7 mol%) at 500°C (▲), 600°C (■) and 700°C (●). Error bars in this plot are from section (Error analysis for titration and CV). The solid lines are the linear regressions.

TABLE 7 | Comparison of slopes of peak current densities *vs*. concentrations of $MgOH^+$(k(T, D)) in molten chlorides determined in this work and reported in the literature (Skar, 2001; Ding et al., 2018b).

T (°C)	k (T, D) (ppm O)/(mA/Cm^2)	Molten chlorides	Data sources
500–700	7.2 ± 2	$MgCl_2$-KCl-NaCl (47/30/23 mol%)	This work
500	38.2 ± 7.6	$MgCl_2$-KCl-NaCl (60/20/20 mol%)	Ding et al. (2018b)
600	13.7 ± 2.7	$MgCl_2$-KCl-NaCl (60/20/20 mol%)	
700	9.4 ± 1.9	$MgCl_2$-KCl-NaCl (60/20/20 mol%)	
728–848	37 ± 8	$MgCl_2$-NaCl (90/10 mol%)	Skar, (2001)
741–842	28 ± 6	$MgCl_2$-NaCl (80/20 mol%)	
730–848	22 ± 4	$MgCl_2$-NaCl (41.5/58.5 mol%)	
730–850	21 ± 6	$MgCl_2$-NaCl (30/70 mol%)	

CV (an electrochemical signal) when it can be calibrated by the *ex situ* measurement. In previous work, it has been repeatedly demonstrated that the density of peak B is linearly related to the concentration of MgOHCl in $MgCl_2$-containing molten chloride salts (Skar, 2001; Ding et al., 2017, 2018b; Choi et al., 2019; Gonzalez et al., 2020; Guo et al., 2021). This work attempted to extend this linear relationship to the tens of ppm O level MgOHCl impurities. All the titration and CV data obtained with *ex situ* and *in situ* measurements are summarized and shown in **Figure 14**, which show the linear relationship between the MgOHCl concentration and the current density of peak B even when the concentration of MgOHCl is low to 39 ppm O. When all the data were between the two error lines, the slope k(T, D) in **Eq. 6** for MgOHCl at 500–700°C was between 5.2 and 9.2 (i.e., 7.2 ± 2) (ppm O)/(mA/cm^2).

Although the linear relationship between MgOHCl and current density in this work is consistent with the literature, the slope k(T, D) obtained in this work is smaller than that in the literature (Skar, 2001; Ding et al., 2017; 2018b) with the same sweep rate of 200 mV/s, as summarized in **Table 7**. This difference may be explained as follows: first, according to **Eq. 6**, the overmeasurement of the MgOHCl concentration, which has been discussed earlier, leads to a larger slope k(T, D). In our previous work (Ding et al., 2017; 2018b), in back titration with 0.1 M HCl (pH = 1), MgO unavoidably reacted with HCl, leading to over-measured concentrations of MgOHCl. In the work of Skar (2001), the concentration of MgOHCl was obtained by combining carbothermal reduction and iodometric titration. The impurities of O_2 or H_2O contained in the salt could also lead to overmeasurement of the O element in carbothermal reduction, further leading to overmeasurement of MgOHCl. Second, according to **Eq. 7**, $k(T, D)$ decreases with the increasing diffusion coefficient (D). As pointed out by Skar (2001), with the increasing $MgCl_2$ content in molten chloride salt, the diffusion coefficient of $MgOH^+$ decreases. The molar fraction of $MgCl_2$ in this work was 47.1 mol%, which is smaller than that in our previous work, which was 60 mol%. Thus, the diffusion coefficient of $MgOH^+$ in this work could be larger than that of our previous work, resulting in a smaller k(T, D). These overlapping factors lead to the difference in the slopes between this work and previous work.

In our previous work, the value of k(T, D) was given separately at the temperatures of 500°C, 600°C, and 700°C. However, in this study, the same value of k(T, D) was obtained at 500–700°C (the key operating temperature range of the molten chloride TES/HTF system), being in line with that of Skar (2001). There are two reasons for giving the same value of k(T, D) in this work. First, when the k(T, D) values were calculated separately, the difference between these values was small. The k(T, D) values were ~7, ~7.5, and ~4 at 500°C, 600°C, and 700°C, respectively. Second, the *in situ* monitoring technique of MgOHCl by CV would be employed as a warning system in the corrosion control system (Villada et al., 2021). Under this condition, the lowest measurable value of MgOHCl concentration is of interest, regardless of the temperature.

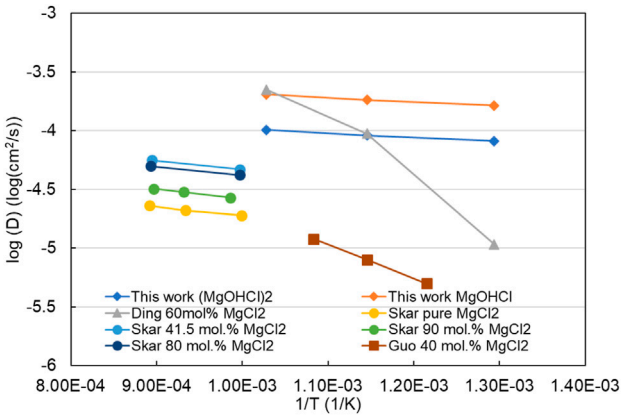

FIGURE 15 | $\log_{10}$(D) *vs*. 1/T of this work and the literature in the melts with different concentrations of $MgCl_2$. "This work MgOHCl and $(MgOHCl)_2$" means that the diffusion coefficients are calculated based on the dissolution form as MgOHCl and $(MgOHCl)_2$ in molten $MgCl_2$-KCl-NaCl with 47.1 mol% $MgCl_2$, respectively.

The diffusion coefficient (D) of MgOHCl can be estimated with the known k(T, D) value and the fixed sweep rate (200 mV/s in this work), according to **Eq. 4** (Berzins–Delahay equation). The estimated diffusion coefficients of MgOHCl in $MgCl_2$-KCl-NaCl at 500°C, 600°C, and 700°C were 1.64 × 10^{-4} cm^2/s, 1.83 × 10^{-4} cm^2/s, and 2.04 × 10^{-4} cm^2/s, respectively. In addition, it was pointed out in the literature (Schenin-King and Picard, 1993; Skar, 2001) that the dissolved MgOHCl in molten chloride salt could be a dimer, i.e., $(MgOHCl)_2$. When the calculation is based

on the dimer $(MgOHCl)_2$, the estimated diffusion coefficients at 500°C, 600°C, and 700°C were 8.20×10^{-5} cm^2/s, 9.14×10^{-5} cm^2/s, and 1.02×10^{-4} cm^2/s, respectively. The Arrhenius relationship ($\log_{10}$(D) *vs*. 1/T) of this work and published data are summarized in a plot, as shown in **Figure 15**. The estimated diffusion coefficients of this work are higher than those in the literature (Skar, 2001; Ding et al., 2018b; Guo et al., 2021), which is mainly caused by the relatively higher k(D, T) adopted in the calculation. Moreover, when the dissolved impurity is considered as the dimer $(MgOHCl)_2$ with two electrons transferred at peak B, the calculated diffusion coefficients are lower than those based on the monomer MgOHCl. In addition, the published diffusion coefficients are estimated by the soluble-soluble Randles–Sevcik equation, while the estimation in this work is based on the soluble-insoluble Berzins–Delahay equation.

CONCLUSION

The $MgCl_2$-KCl-NaCl molten salt shows low corrosivity to the metallic structural materials (i.e., alloys) at ≥700°C when the concentration of the main corrosive impurity MgOHCl is as low as tens of ppm O. To allow the use of inexpensive alloys (e.g. stainless steels) for TES/HTF with $MgCl_2$-KCl-NaCl molten salt at ≥700°C, the salt impurity needs to be controlled at the tens of ppm O level by using the corrosion control system (CCS), including the online corrosion monitoring subsystem and corrosion mitigation subsystem. Thus, reliable chemical analysis and monitoring techniques of MgOHCl at the tens of ppm O level are vital in CCS to ensure its effectiveness, efficiency, and economics.

This work developed a chemical analysis technique based on direct titration and a high-precision automatic titrator, which can measure MgOHCl at the tens of ppm O level, e.g., 36 ppm O MgOHCl with a measurement error of about 7 ppm O. This chemical analysis technique was used to calibrate the *in situ* monitoring technique based on the CV developed in our previous work. The obtained CV data (i.e., peak current density) for 500–700°C shows good linearity with the data on direct titration (i.e., MgOHCl concentration) in the range from 39 to 4211 ppm O. The slope of the concentration of MgOHCl vs. the peak current density in CV was 7.2 ±2 (ppm O)/(mA/cm^2) at 500–700°C. Using the calibrated CV technique and the slope in CCS, the corrosive impurity of MgOHCl low to tens of ppm O could be monitored *in situ* with quick response and cost-effectively. With the slope value, the estimated diffusion coefficients of MgOHCl in $MgCl_2$-KCl-NaCl at 500–700°C were 1.64×10^{-4}–2.04×10^{-4} cm^2/s, when it is assumed that the existing form of MgOHCl is the monomer $MgOH^+$.

The two techniques for MgOHCl measurement developed in this work could be used to develop an *in situ* corrosion control system to ensure the long service time of the molten chloride TES/HTF system in next-generation CSP plants. Some future work is suggested to realize the commercial application of these techniques:

- the design of the *in situ* monitoring subsystem based on CV including the electrodes and their material selection,
- building a molten chloride test loop and testing the CV technique and subsystem under dynamic conditions of molten chlorides close to the real application conditions,
- testing the chemical analysis technique for the salt samples from the loop test, and
- development and testing of the corrosion mitigation techniques studied in our previous work or available in the literature in the molten chloride test loop.

DATA AVAILABILITY STATEMENT

The original contributions presented in the study are included in the article/supplementary material; further inquiries can be directed to the corresponding authors.

AUTHOR CONTRIBUTIONS

WD, QG, and YC contributed to the conception and design of the study. QG, WD, and JS performed the statistical analysis. QG wrote the first draft of the manuscript. All authors contributed to manuscript revision, read, and approved the submitted version.

ACKNOWLEDGMENTS

This research has been performed within the DLR-DAAD fellowship program (Nr. 57540125). The authors would like to thank the colleagues M. Braun, R. Hoffmann, and A. Hanke for technical support in the different laboratories.

REFERENCES

Berzins, T., and Delahay, P. (1953). Oscillographic Polarographic Waves for the Reversible Deposition of Metals on Solid Electrodes. *J. Am. Chem. Soc.* 75 (3), 555–559. doi:10.1021/ja01099a013

Boghosian, S., Godø, A., Mediaas, H., Ravlo, W., and Østvold, T. (1991). Oxide Complexes in Alkali--Alkaline-Earth Chloride Melts. *Acta Chem. Scand.* 45, 145–157. doi:10.3891/acta.chem.scand.45-0145

Chen, Y., An, Z., and Chen, M. (2018). Competition Mechanism Study of Mg+H2O and MgO+H2O Reaction. *IOP Conf. Ser. Mat. Sci. Eng.* 394, 022015. doi:10.1088/1757-899x/394/2/022015

Choi, S., Orabona, N. E., Dale, O. R., Okabe, P., Inman, C., and Simpson, M. F. (2019). Effect of Mg Dissolution on Cyclic Voltammetry and Open Circuit Potentiometry of Molten MgCl2-KCl-NaCl Candidate Heat Transfer Fluid for Concentrating Solar Power. *Sol. Energy Mater. Sol. Cells* 202, 110087. doi:10.1016/j.solmat.2019.110087

Ding, W., Bonk, A., and Bauer, T. (2018a). Corrosion Behavior of Metallic Alloys in Molten Chloride Salts for Thermal Energy Storage in Concentrated Solar Power Plants: A Review. *Front. Chem. Sci. Eng.* 12 (3), 564–576. doi:10.1007/s11705-018-1720-0

Ding, W., Bonk, A., Gussone, J., and Bauer, T. (2017). Cyclic Voltammetry for Monitoring Corrosive Impurities in Molten Chlorides for Thermal Energy Storage. *Energy Procedia* 135, 82–91. doi:10.1016/j.egypro.2017.09.489

Ding, W., Bonk, A., Gussone, J., and Bauer, T. (2018b). Electrochemical Measurement of Corrosive Impurities in Molten Chlorides for Thermal Energy Storage. *J. Energy Storage* 15, 408–414. doi:10.1016/j.est.2017.12.007

Ding, W., Gomez-Vidal, J., Bonk, A., and Bauer, T. (2019a). Molten Chloride Salts for Next Generation CSP Plants: Electrolytical Salt Purification for Reducing Corrosive Impurity Level. *Sol. Energy Mater. Sol. Cells* 199, 8–15. doi:10.1016/j.solmat.2019.04.021

Ding, W., Shi, H., Jianu, A., Xiu, Y., Bonk, A., Weisenburger, A., et al. (2019b). Molten Chloride Salts for Next Generation Concentrated Solar Power Plants: Mitigation Strategies against Corrosion of Structural Materials. *Sol. Energy Mater. Sol. Cells* 193, 298–313. doi:10.1016/j.solmat.2018.12.020

Ding, W., Shi, H., Xiu, Y., Bonk, A., Weisenburger, A., Jianu, A., et al. (2018c). Hot Corrosion Behavior of Commercial Alloys in Thermal Energy Storage Material of Molten MgCl2/KCl/NaCl under Inert Atmosphere. *Sol. Energy Mater. Sol. Cells* 184, 22–30. doi:10.1016/j.solmat.2018.04.025

Ding, W., Yang, F., Bonk, A., and Bauer, T. (2021). Molten Chloride Salts for High-Temperature Thermal Energy Storage: Continuous Electrolytic Salt Purification with Two Mg-Electrodes and Alternating Voltage for Corrosion Control. *Sol. Energy Mater. Sol. Cells* 223, 110979. doi:10.1016/j.solmat.2021.110979

Dong, C., Cairney, J., Sun, Q., Maddan, O. L., He, G., and Deng, Y. (2010). Investigation of Mg(OH)2 Nanoparticles as an Antibacterial Agent. *J. Nanopart Res.* 12 (6), 2101–2109. doi:10.1007/s11051-009-9769-9

Fruhwirth, O., Herzog, G. W., Hollerer, I., and Rachetti, A. (1985). Dissolution and Hydration Kinetics of MgO. *Surf. Technol.* 24 (3), 301–317. doi:10.1016/0376-4583(85)90080-9

Gilardi, T., Rodriguez, G., Gomez, A., Leybros, J., Borgard, J., Carles, P., et al. (2006). "Influence of Material Choice on Cost Estimation of Some Key Components of the Sulfur Iodine Thermochemical Process," in Proc. of 16th World Hydrogen Energy Conference (WHEC), 13-16 June 2006 (Lyon, France: Association Francaise pour l'Hydrogene et les Piles a Combustible AFHYPAC), 13–16.

Gonzalez, M., Faulkner, E., Zhang, C., Choi, S., and Simpson, M. F. (2020). Electrochemical Methods for Analysis of Hydroxide and Oxide Impurities in Li, Mg/Na, and Ca Based Molten Chloride Salts. *ECS Trans.* 98 (10), 161–169. doi:10.1149/09810.0161ecst

Grégoire, B., Oskay, C., Meißner, T. M., and Galetz, M. C. (2020). Corrosion Mechanisms of Ferritic-Martensitic P91 Steel and Inconel 600 Nickel-Based Alloy in Molten Chlorides. Part II: NaCl-KCl-MgCl2 Ternary System. *Sol. Energy Mater. Sol. Cells* 216, 110675. doi:10.1016/j.solmat.2020.110675

Guo, J., Hoyt, N., and Williamson, M. (2021). Multielectrode Array Sensors to Enable Long-Duration Corrosion Monitoring and Control of Concentrating Solar Power Systems. *J. Electroanal. Chem.* 884, 115064. doi:10.1016/j.jelechem.2021.115064

Kashani-Nejad, S., Ng, K.-W., and Harris, R. (2005). MgOHCl Thermal Decomposition Kinetics. *Metall Materi Trans B* 36 (1), 153–157. doi:10.1007/s11663-005-0015-2

Kashani-Nejad, S. (2005). Oxides in the Dehydration of Magnesium Chloride Hexahydrate. Montreal, Canada: McGill University. Thesis.

Kipouros, G. J., and Sadoway, D. R. (2001). A Thermochemical Analysis of the Production of Anhydrous MgCl2. *J. Light Metals* 1 (2), 111–117. doi:10.1016/S1471-5317(01)00004-9

Klammer, N., Engtrakul, C., Zhao, Y., Wu, Y., and Vidal, J. (2020). Method to Determine MgO and MgOHCl in Chloride Molten Salts. *Anal. Chem.* 92 (5), 3598–3604. doi:10.1021/acs.analchem.9b04301

Kurley, J. M., Halstenberg, P. W., McAlister, A., Raiman, S., Dai, S., and Mayes, R. T. (2019). Enabling Chloride Salts for Thermal Energy Storage: Implications of Salt Purity. *RSC Adv.* 9 (44), 25602–25608. doi:10.1039/c9ra03133b

Mehos, M., Turchi, C., Vidal, J., Wagner, M., Ma, Z., Ho, C., et al. (2017). *Concentrating Solar Power Gen3 Demonstration Roadmap*. Golden, CO (United States): United States: National Renewable Energy Lab.NREL.

Randles, J. E. B. (1948). A Cathode Ray Polarograph. Part II.-The Current-Voltage Curves. *Trans. Faraday Soc.* 44, 327–338. doi:10.1039/tf9484400327

Schenin-King, J., and Picard, G. (1993). "Oxoacidity Effect on Metallic Oxide Dissolution Reactions in Fused Chlorides," in Retrospective Collection*: Trans Tech Publ)* (Durnten, Switzerland: Publisher and Materials Science and Enginerring), 13–24.

Ševčík, A. (1948). Oscillographic Polarography with Periodical Triangular Voltage. *Collect. Czechoslov. Chem. Commun.* 13, 349–377.

Skar, R. A. (2001). *Chemical and Electrochemical Characterisation of Oxide/hydroxide Impurities in the Electrolyte for Magnesium Production*. Trondheim, Norway: Norwegian University of Science and Technology Fakultet for naturvitenskap og teknologi.

Song, J., Huang, X., Fan, Y., Yi, J., Shu, Y., and He, J. (2018). *In Situ* Monitoring of O2–Concentration in Molten NaCl-KCl at 750°C. *J. Electrochem. Soc.* 165 (5), E245–E249. doi:10.1149/2.1101805jes

Sun, H., Wang, J.-Q., Tang, Z., Liu, Y., and Wang, C. (2020). Assessment of Effects of Mg Treatment on Corrosivity of Molten NaCl-KCl-MgCl2 Salt with Raman and Infrared Spectra. *Corros. Sci.* 164, 108350. doi:10.1016/j.corsci.2019.108350

Sun, H., Wang, J., Li, Z., Zhang, P., and Su, X. (2018). Corrosion Behavior of 316SS and Ni-Based Alloys in a Ternary NaCl-KCl-MgCl2 Molten Salt. *Sol. Energy* 171, 320–329. doi:10.1016/j.solener.2018.06.094

Turchi, C. S., Vidal, J., and Bauer, M. (2018). Molten Salt Power Towers Operating at 600-650 °C: Salt Selection and Cost Benefits. *Sol. Energy* 164, 38–46. doi:10.1016/j.solener.2018.01.063

Villada, C., Ding, W., Bonk, A., and Bauer, T. (2021). Engineering Molten MgCl2-KCl-NaCl Salt for High-Temperature Thermal Energy Storage: Review on Salt Properties and Corrosion Control Strategies. *Sol. Energy Mater. Sol. Cells* 232, 111344. doi:10.1016/j.solmat.2021.111344

Williams, T., Shum, R., and Rappleye, D. (2021). Review-Concentration Measurements in Molten Chloride Salts Using Electrochemical Methods. *J. Electrochem. Soc.* 168 (12), 123510. doi:10.1149/1945-7111/ac436a

Zhang, M., Ge, J., Yin, T., and Zhang, J. (2020). Redox Potential Measurements of Cr(II)/Cr Ni(II)/Ni and Mg(II)/Mg in Molten MgCl2-KCl-NaCl Mixture. *J. Electrochem. Soc.* 167 (11), 116505. doi:10.1149/1945-7111/aba15a

Zhao, Y. (2020). *Molten Chloride Thermophysical Properties, Chemical Optimization, and Purification*. Golden, CO (United States): National Renewable Energy Lab.NREL.

Conflict of Interest: The authors declare that the research was conducted in the absence of any commercial or financial relationships that could be construed as a potential conflict of interest.

Publisher's Note: All claims expressed in this article are solely those of the authors and do not necessarily represent those of their affiliated organizations, or those of the publisher, the editors, and the reviewers. Any product that may be evaluated in this article, or claim that may be made by its manufacturer, is not guaranteed or endorsed by the publisher.